Preconditioned flow as a solution to the hierarchical growth problem in the generalized Lefschetz thimble method

Jun NISHIMURA[1,2)∗], Katsuta SAKAI[1,3)†] and Atis YOSPRAKOB[2,4)‡]

[1)]*KEK Theory Center, Institute of Particle and Nuclear Studies,*
High Energy Accelerator Research Organization,
1-1 Oho, Tsukuba, Ibaraki 305-0801, Japan
[2)]*Graduate Institute for Advanced Studies, SOKENDAI,*
1-1 Oho, Tsukuba, Ibaraki 305-0801, Japan
[3)]*College of Liberal Arts and Sciences, Tokyo Medical and Dental University,*
2-8-30 Kounodai, Ichikawa, Chiba 272-0827, Japan
[4)]*Department of Physics, Niigata University,*
8050 Igarashi 2-no-cho, Nishi-ku, Niigata-shi, Niigata 950-2181, Japan

Abstract

The generalized Lefschetz thimble method is a promising approach that attempts to solve the sign problem in Monte Carlo methods by deforming the integration contour using the flow equation. Here we point out a general problem that occurs due to the property of the flow equation, which extends a region on the original contour exponentially to a region on the deformed contour. Since the growth rate for each eigenmode is governed by the singular values of the Hessian of the action, a huge hierarchy in the singular value spectrum, which typically appears for large systems, leads to various technical problems in numerical simulations. We solve this hierarchical growth problem by preconditioning the flow so that the growth rate becomes identical for every eigenmode. As an example, we show that the preconditioned flow enables us to investigate the real-time quantum evolution of an anharmonic oscillator with the system size that can hardly be achieved by using the original flow.

[∗]E-mail address : jnishi@post.kek.jp

[†]E-mail address : sakai.las@tmd.ac.jp

[‡]E-mail address : ayosp@phys.sc.niigata-u.ac.jp

1   Introduction

In theoretical physics, we are often faced with a system which cannot be solved analytically. In that case, we have to either perform perturbative calculations by taking some limits in the parameter space, or make some plausible simplifications so that the system becomes analytically tractable. Such approximations, however, quite often obscure the physics we are most interested in. In this regard, numerical simulation is of particular importance since it provides us with a powerful tool to investigate various systems nonperturbatively from first principles without such approximations.

Here we are concerned with numerical simulation of multi-variable integrals with some weight, where the number of variables N representing the system size is large. In the case with a positive-definite weight such as the Boltzmann weight that appears in classical statistical mechanics, the numerical integration can be realized by Monte Carlo (MC) simulation based on the importance sampling, where we interpret the weight as the probability distribution. However, we often encounter a weight $w = e^{-S}$ with a complex action S, which cannot be interpreted as the probability distribution. A naive prescription is the so-called reweighting, where we interpret the absolute value of the weight as the probability distribution, and take into account the phase factor when we take the average of the observables. This does not really work for large systems since the phase factor oscillates violently depending on the generated configurations, which leads to huge cancellations among them. Thus, in order to obtain the correct expectation value, one needs a huge number of configurations, which typically grows exponentially with the system size N. This is the notorious sign problem, which has been hindering nonperturbative studies of various important systems, such as finite density QCD, theories with a θ-term, strongly correlated electron systems, and the Lorentzian path integrals for the real-time quantum evolution.

In the last decade, various new approaches have been developed to overcome the sign problem. In particular, within the framework of MC methods, two promising approaches, the complex Langevin method [1, 2] and the Lefschetz thimble method [3, 4, 5, 6] have been studied intensively[1]. A common feature of these two approaches is that one complexifies the variables and extends the weight and the observables as holomorphic functions of the complexified variables. In the complex Langevin method, one generates complexified configurations using the Langevin equation with the drift term given by the gradient of the action.

---

[1]As a promising approach without MC simulation, the tensor renormalization group has been developed [7, 8, 9, 10, 11]. The basic idea is to rewrite the integral as a network of tensors and to perform a coarse-graining procedure iteratively using the singular value decomposition. Since there is no need to interpret the weight as the probability distribution, the method is free from the sign problem from the outset.

While the cost of this method is O(N) as in typical MC simulation, it is applicable only to a limited class of systems due to the conditions for justification [12, 13, 14, 15, 16, 17, 18].

On the other hand, the Lefschetz thimble method is based on the Picard-Lefschetz theory, in which one deforms the integration contour in the complex space to a set of steepest descent paths emanating from some saddle points of the action. These paths are called the Lefschetz thimbles (or thimbles in short). The phase of the complex weight is constant along each thimble, and the sign problem is solved as far as the phase factor coming from the integration measure can be taken into account by reweighting [6].

In practice, the contour deformation can be realized by solving the so-called anti-holomorphic gradient flow equation for the variables [19], where the amount of flow (the flow time) plays the role of the deformation parameter. While the Lefschetz thimbles are obtained in the long flow time limit, one can also use a deformed contour obtained at finite flow time of the order of $\log N$, which is expected to be long enough to solve the sign problem for the system size N. This is called the generalized thimble method (GTM), which has a big advantage over the original Lefschetz thimble method in that it does not require prior knowledge of the Lefschetz thimbles. (See Ref. [20] for a review.)

When there are more than one thimbles that contribute to the integral, the GTM suffers from an ergodicity problem for a large flow time due to the infinite potential barriers between different thimbles. For a relatively small system, one can just choose the flow time long enough to solve the sign problem but not too long so that the ergodicity problem can be avoided [19]. The range of the flow time that can avoid both problems, however, shrinks as the system size increases and eventually vanishes. In order to solve both problems even in that case, one can integrate over the flow time[2], which amounts to treating the flow time as an extra dynamical variable in the simulation [24, 25].

As an efficient algorithm for numerical simulations in general, the Hybrid Monte Carlo (HMC) algorithm is widely used. In this algorithm, one uses a fictitious Hamilton dynamics to update the configuration. When one applies this algorithm to the GTM, there are actually two approaches depending on whether one considers the Hamilton dynamics on the deformed contour or on the original contour. In the first approach, one has to solve the Hamilton dynamics of a constrained system in order to make sure that the configuration remains on the deformed contour [6, 23]. This requires some complicated calculations since the deformed contour is given only implicitly by solving the gradient flow equation. A big advantage of this approach, however, is that the probability distribution of the generated configurations automatically includes the modulus of the Jacobian associated with the flow

---

[2]This proposal is a significant improvement over the related ones [21, 22, 23] based on tempering with respect to the flow time, which requires the calculation of the Jacobian when one swaps the replicas.

of variables, which is not the case in the second approach as we explain below.

In the second approach, one can just solve the Hamilton dynamics of an unconstrained system on the real axis, which makes this part of the algorithm much simpler than in the first approach. The force term of the Hamilton equation has to be calculated by taking the derivative of the action on the deformed contour with respect to the variables on the real axis, which is actually possible without large computational cost if one uses the idea of backpropagation [26]. A drawback of this second approach, however, is that the probability distribution of the generated configurations does not include the modulus of the Jacobian associated with the flow of variables, and therefore it has to be included by reweighting together with the phase of the Jacobian. In fact, the modulus may fluctuate considerably depending on the generated configurations. In that case, only a few configurations that have a large modulus of the Jacobian dominate the ensemble, and one cannot increase the statistics efficiently. This is the so-called overlap problem that can occur in general when one uses reweighting. In what follows, we call these two approaches the on-thimble approach[3] and the on-axis approach, respectively.

In this paper, we point out a general problem that occurs when the GTM is applied to large systems. In the GTM, the deformation of the integration contour by the gradient flow equation is really the key to solve the sign problem. The crucial feature of the gradient flow equation that makes this possible is that it maps a small region on the real axis to an exponentially large region on the deformed contour as the flow time becomes longer. The growth rate of this exponential behavior, however, depends on the eigenmode, and it is governed by the singular values of the Hessian of the action. As the system size increases, the singular value spectrum typically exhibits a huge hierarchy. As a consequence, if we choose the flow time long enough to solve the sign problem associated with the eigenmodes corresponding to small singular values, the eigenmodes corresponding to large singular values tend to diverge and easily get out of control[4].

We show that this hierarchical growth problem of the GTM can be solved by preconditioning the gradient flow equation. For that, we first point out that we are free to introduce a Hermitian positive-definite kernel on the right-hand side of the gradient flow equation without spoiling its property that is necessary to solve the sign problem. One can actually use this freedom to make the growth rate identical for every eigenmode, which implies

---

[3]This is a bit of abuse of the word "thimble" since here it actually represents a deformed contour obtained by the gradient flow at finite τ.

[4]This problem should not be confused with the blow-up problem of the flow equation discussed in Ref. [27], which occurs when the integrand becomes zero at some point in the complexified configuration space. In fact, we consider that the blow-up problem does not occur if one uses the preconditioned flow that we propose in this paper as we discuss in Appendix A.

that the hierarchical growth problem can be solved by the preconditioned flow. Moreover, when applied to the on-axis approach, the preconditioned flow suppresses the fluctuation of the Jacobian, which can otherwise cause the overlap problem as we mentioned above. Actual implementation of this preconditioned flow can be done by using the techniques developed for Rational Hybrid Monte Carlo algorithm, which is widely used in numerical simulation. In order to demonstrate how the preconditioning works, we apply the GTM to the real-time quantum evolution of an anharmonic oscillator[5]. In particular, we show that the preconditioning enables us to simulate a large system that cannot be achieved otherwise. We also show that the computational cost for generating configurations grows only linearly with the system size N for a local system if we implement the preconditioning in the flow appropriately. Preliminary discussions on the precondition flow are presented in our previous paper [33] and a proceedings article [34], where we establish a new picture of quantum tunneling in the real-time path integral using the GTM.

The rest of this paper is organized as follows. In Section 2, we discuss the hierarchical growth problem of the original flow due to the hierarchy in the singular value spectrum of the Hessian. In particular, we show that the problem becomes severer when the system size increases using a simple example of a harmonic oscillator. In Section 3, we explain our proposal of the preconditioned flow equation, and discuss how it can be implemented in practice. In Section 4, we demonstrate how the preconditioning solves the hierarchical growth problem of the flow as well as the overlap problem in the on-axis approach by applying the GTM to the real-time quantum evolution of an anharmonic oscillator. Section 5 is devoted to a summary and discussions. In Appendix A, we discuss the absence of the so-called blow-up problem in the preconditioned flow. In Appendix B, we show that the preconditioned flow actually changes the thimble and yet it solves the sign problem using a simple example. In Appendix C, we provide a brief review on the application of the HMC to the GTM based on the on-axis approach. In Appendix D, we discuss how the idea of backpropagation for calculating the force term in the HMC algorithm works with the preconditioned flow. In Appendix E, we present the parameters of the GTM used in our simulations.

2   The hierarchical growth problem in the GTM

In this section, we discuss the crucial properties of the gradient flow equation that make it possible to solve the sign problem. In particular, we show that it maps a region on the

---

[5]See also Refs. [28, 29, 30, 31, 32] for calculations of the real-time quantum evolution using the GTM based on the Schwinger-Keldysh formalism, which actually simplifies the simulation [30].

real axis to a region on the deformed contour, which becomes exponentially large with the flow time. Moreover the growth rate for each eigenmode is governed by the singular value spectrum of the Hessian of the action. When the system size N is large, the growth rate tends to exhibit a large hierarchy, which is the hierarchical growth problem.

2.1 Hierarchical growth property of the flow equation

Let us consider a partition function with a complex action $S(x) \in \mathbb{C}$ defined by

$$Z = \int_{\mathbb{R}^N} d^N x \, e^{-S(x)} \,. \tag{2.1}$$

In the GTM, one deforms the integration contour by using the gradient flow equation

$$\frac{dz_j(\sigma)}{d\sigma} = \overline{\frac{\partial S(z(\sigma))}{\partial z_j}} \,. \tag{2.2}$$

By solving this equation from $\sigma = 0$ to $\sigma = \tau$ with the initial condition $z_j(0) = x_j$, we obtain a map $x \mapsto z(x, \tau) \equiv z(\tau)$. Then the deformed contour is defined by $\Sigma_\tau = \{z(x, \tau) | x \in \mathbb{R}^N\}$, where τ is the so-called flow time. Due to Cauchy's theorem, the partition function can be rewritten as

$$Z = \int_{\Sigma_\tau} d^N z \, e^{-S(z)} \,. \tag{2.3}$$

The crucial property of the flow equation is

$$\frac{dS(z(\sigma))}{d\sigma} = \frac{\partial S(z(\sigma))}{\partial z_j} \frac{dz_j(\sigma)}{d\sigma} = \left| \frac{\partial S(z(\sigma))}{\partial z_j} \right|^2 > 0 \,, \tag{2.4}$$

which implies that $\operatorname{Re} S(z(\sigma))$ increases monotonically with increasing σ, while $\operatorname{Im} S(z(\sigma))$ remains constant. In the infinite flow time limit $\tau = \infty$, the deformed contour Σ_∞ is composed of a set of Lefschetz thimbles. Each thimble can be obtained by the flow from some saddle point (defined by $\frac{\partial S(z)}{\partial z_j} = 0$), and hence $\operatorname{Re} S(z(\sigma))$ increases monotonically keeping $\operatorname{Im} S(z)$ constant as one flows away from the saddle point. This implies that the sign problem is solved on each thimble as far as the phase factor coming from the integration measure $d^N z$ in (2.3) can be treated by reweighting [6]. The key mechanism for solving the sign problem here is that there is some point P on $\mathbb{R}^N$ which flows into a saddle point in the $\tau \to \infty$ limit, and the thimble associated with that saddle point is obtained by mapping an infinitesimal vicinity of the point P using the flow. This property of the flow, together with the fact that $\operatorname{Im} S(z)$ is kept constant along the flow, makes it possible to solve the

sign problem. In fact, the sign problem can be solve even at finite τ as far as τ is large enough to suppress the fluctuation of $\operatorname{Im} S(z)$.

Here we discuss in more detail how a small region on the original contour $\mathbb{R}^N$ is extended in the deformed contour. For that, let us consider two points x and $x + \delta x$ on the real axes, which differ only by some infinitesimal displacement δx. The displacement $\zeta(\sigma) \equiv z(x + \delta x, \sigma) - z(x, \sigma)$ of the two points after some flow time σ is given by the equation

$$\frac{d\zeta_j(\sigma)}{d\sigma} = \overline{H_{jk}(z(\sigma))\, \zeta_k(\sigma)} \tag{2.5}$$

with $\zeta_j(0) = \delta x_j$, where H is the Hessian of the action defined by

$$H_{ij}(z) = \frac{\partial^2 S(z)}{\partial z_i \partial z_j} \ . \tag{2.6}$$

In order to solve (2.5), let us rewrite it as

$$\frac{d}{d\sigma} \begin{pmatrix} \zeta(\sigma) \\ \bar{\zeta}(\sigma) \end{pmatrix} = \mathcal{H}(\sigma) \begin{pmatrix} \zeta(\sigma) \\ \bar{\zeta}(\sigma) \end{pmatrix} \ , \tag{2.7}$$

where we use the vector notation $\zeta = (\zeta_1, \cdots, \zeta_N)^\top$, $\bar{\zeta} = (\bar{\zeta}_1, \cdots, \bar{\zeta}_N)^\top$ and define the $2N \times 2N$ Hermitian[6] matrix $\mathcal{H}(\sigma)$ as

$$\mathcal{H}(\sigma) = \begin{pmatrix} & \overline{H(z(\sigma))} \\ H(z(\sigma)) & \end{pmatrix} \ . \tag{2.8}$$

Thus the solution to the differential equation (2.5) can be written down formally as

$$\begin{pmatrix} \zeta(\tau) \\ \bar{\zeta}(\tau) \end{pmatrix} = \mathcal{P} \exp \left(\int_0^\tau d\sigma \, \mathcal{H}(\sigma) \right) \begin{pmatrix} \delta x \\ \delta x \end{pmatrix} \ , \tag{2.9}$$

where $\delta x = (\delta x_1, \cdots, \delta x_N)^\top$ and $\mathcal{P} \exp$ represents the path-ordered exponential, which ensures that $\mathcal{H}(\sigma)$ with smaller σ comes on the right after Taylor expansion.

In order to understand the behavior of the solution (2.9), let us diagonalize the Hermitian matrix $\mathcal{H}(\sigma)$. For that, we consider the singular value decomposition (SVD) of the Hessian $H_{ij}(z(\sigma))$ given as[7]

$$H(z(\sigma)) = U^\top(\sigma)\, \Lambda(\sigma)\, U(\sigma) \ , \tag{2.10}$$

---

[6]Note that the Hessian is symmetric $H^\top = H$ and hence $\bar{H} = H^\dagger$.

[7]This is known as the Takagi decomposition, which is the SVD for a complex symmetric matrix.

where U is a unitary matrix and $\Lambda = \text{diag}(\lambda_1, \cdots, \lambda_N)$ is a real diagonal matrix with positive[8] entries $\lambda_j > 0$. Using $\Lambda(\sigma)$ and $U(\sigma)$, we can diagonalize $\mathcal{H}(\sigma)$ as

$$\mathcal{H}(\sigma) = \mathcal{U}^\dagger(\sigma) \begin{pmatrix} \Lambda(\sigma) & \\ & -\Lambda(\sigma) \end{pmatrix} \mathcal{U}(\sigma) , \tag{2.11}$$

$$\mathcal{U}(\sigma) = \frac{1}{\sqrt{2}} \begin{pmatrix} \mathbf{1}_N & \mathbf{1}_N \\ -\mathbf{1}_N & \mathbf{1}_N \end{pmatrix} \begin{pmatrix} U(\sigma) & \\ & \overline{U}(\sigma) \end{pmatrix} . \tag{2.12}$$

This implies that the displacement grows exponentially with σ for a small region of σ, in which $H_{jk}(z(\sigma))$ can be regarded as constant. Moreover, the growth rate is governed by the singular values of the Hessian $H(z)$, and it depends on the eigenmode $\zeta_{\text{E}}^{(i)} = \text{Re}(U_{ij}\zeta_j) \sim e^{\lambda_i \sigma}$. When the singular value spectrum has a large hierarchy, the growth rate becomes very different for different eigenmodes. Since the flow time τ is common to all the eigenmodes, if we choose τ in such a way that the sign problem is solved for the eigenmodes $\zeta_{\text{E}}^{(i)}$ with small λ_i, the eigenmodes $\zeta_{\text{E}}^{(i)}$ with large λ_i tend to diverge.

This problem is severer in the on-axis approach since one has to update the configuration on the real axis. In order to avoid the hierarchical growth problem, one has to choose a very small step size in solving the Hamilton dynamics of the HMC algorithm, which makes the simulation extremely slow. In the case of the on-thimble approach, one updates the configuration on the deformed contour directly, but the problem may occur when one solves the flow equation to ensure that the updated configuration is still on the deformed contour. (See Section 5 for further discussions.)

2.2 Example of a harmonic oscillator

In this section, we show that the hierarchical growth problem discussed in the previous section indeed occurs in a simple example of a harmonic oscillator. This example provides a clear understanding of the problem since the gradient flow equation can be solved explicitly.

The path integral that describes the real-time quantum evolution of a harmonic oscillator is given by (2.1) with the action

$$S = -i \sum_{j=0}^{N} \epsilon \left\{ \frac{1}{2} \left(\frac{x_{j+1} - x_j}{\epsilon} \right)^2 - \frac{1}{2} m^2 \frac{x_{j+1}^2 + x_j^2}{2} \right\} , \tag{2.13}$$

where we fix $x_0 = x_{N+1} = 0$ for simplicity and treat $x_1, \cdots, x_N$ as variables. The path integral (2.1) then represents the transition amplitude from the origin to the origin in time $T = \epsilon(N+1)$ up to some known normalization factor.

---

[8]Here we assume that there are no zero singular values for simplicity. However, our idea can be easily extended to the case in which this assumption does not hold. See footnote 13.

In this example, the Hessian $H(z)$ of the action defined by (2.6) is a constant matrix, which does not depend on the complexified configuration z_j. Furthermore, it is not only symmetric but also pure imaginary. Therefore, we can diagonalize it as

$$H = -i\, O^\top \tilde{\Lambda}\, O \ , \tag{2.14}$$

where $O \in \mathrm{SO}(N)$ and $\tilde{\Lambda}$ is a real diagonal matrix $\tilde{\Lambda} = \mathrm{diag}(\tilde{\lambda}_1, \cdots, \tilde{\lambda}_N)$ with

$$\tilde{\lambda}_j = \epsilon \left\{ \frac{4}{\epsilon^2} \sin^2 \frac{\pi j}{2(N+1)} - m^2 \right\} \ . \tag{2.15}$$

Note that $\tilde{\lambda}_j$ can be negative in general, and the singular values[9] are given by $\lambda_j = |\tilde{\lambda}_j|$.

Using the Hessian H and its diagonalized form (2.14), the action can be written as

$$S = \frac{1}{2} x_j H_{jk} x_k = -\frac{i}{2} \sum_{j=1}^N \tilde{\lambda}_j (y_j)^2 \ , \tag{2.16}$$

where we have defined the variables $y_j = O_{jk} x_k$. Thus the integral (2.1) is rewritten as

$$Z = \int_{\mathbb{R}^N} d^N y \ \exp\left(\frac{i}{2} \sum_{j=1}^N \tilde{\lambda}_j\, y_j^2 \right) \ . \tag{2.17}$$

The flow equation for the complexified variables $z_j(y, \tau)$ is given by

$$\frac{\partial z_j(y, \sigma)}{\partial \sigma} = i \tilde{\lambda}_j \overline{z_j(y, \sigma)} \ , \tag{2.18}$$

$$z_j(y, 0) = y_j \ , \tag{2.19}$$

whose solution can be readily obtained as

$$z_j(y, \sigma) = \left\{ \cosh(\tilde{\lambda}_j \sigma) + i \sinh(\tilde{\lambda}_j \sigma) \right\} y_j \ . \tag{2.20}$$

Note that the gradient flow magnifies the displacement δy_j on the real axis by a factor of

$$R_j(\sigma) \equiv \sqrt{\cosh^2(\tilde{\lambda}_j \sigma) + \sinh^2(\tilde{\lambda}_j \sigma)} = \sqrt{\cosh(2\tilde{\lambda}_j \sigma)} \sim e^{\lambda_j \sigma} \ , \tag{2.21}$$

which grows exponentially with σ, and the growth rate is given by the singular value $\lambda_j = |\tilde{\lambda}_j|$ as suggested by the general discussion in the previous section.

---

[9]The singular value decomposition (2.10) of $H = U^\top \Lambda\, U$ is given by $U = V O$, where V is a diagonal unitary matrix with the entries given by either $e^{\frac{\pi}{4} i}$ or $e^{-\frac{\pi}{4} i}$ depending on whether the corresponding eigenvalue $\tilde{\lambda}_j$ is negative or positive, respectively.

Using (2.20), the integral on the deformed contour is written as

$$Z = \int_{\Sigma_\tau} d^N z \, \exp\left(\frac{i}{2} \sum_{j=1}^N \tilde{\lambda}_j \, z_j^2 \right) \tag{2.22}$$

$$= \int_{\mathbb{R}^N} d^N y \, \det J \, \exp\left(-\frac{1}{2} \sum_{j=1}^N \tilde{\lambda}_j \left\{ \sinh(2\tilde{\lambda}_j \tau) - i \right\} y_j^2 \right) . \tag{2.23}$$

Here the Jacobi matrix J associated with the deformation of the contour is given by

$$J_{jk} = \frac{\partial z_j(y,\tau)}{\partial y_k} = \left\{ \cosh(\tilde{\lambda}_j \tau) + i \sinh(\tilde{\lambda}_j \tau) \right\} \delta_{jk} , \tag{2.24}$$

which is independent of y and hence can be factored out of the integral.

From (2.23), one can see how the sign problem is solved by increasing τ. The real part of the argument of the exponential function implies that the region of y_j that contribute to the integral is $|y_j| \lesssim \Delta_j$, where

$$\Delta_j = \left\{ \tilde{\lambda}_j \sinh(2\tilde{\lambda}_j \tau) \right\}^{-1/2} . \tag{2.25}$$

In that region, the phase factor of the integrand is close to unity as far as

$$\frac{1}{2} |\tilde{\lambda}_j| (\Delta_j)^2 \ll \pi . \tag{2.26}$$

Combining (2.25) and (2.26), the sign problem associated with the eigenmode j is solved if

$$\tau \gg \frac{1}{2\lambda_j} \operatorname{arcsinh}\left(\frac{1}{2\pi} \right) . \tag{2.27}$$

Thus, in order to solve the sign problem of the whole system, one has to satisfy (2.27) for the smallest singular value $\lambda_{\min}$. In that case, the magnification factor (2.21) for the largest singular value $\lambda_{\max}$ becomes

$$R_{\max}(\tau) \sim \exp\left(c \frac{\lambda_{\max}}{\lambda_{\min}} \right) , \tag{2.28}$$

$$c \gg \frac{1}{2} \operatorname{arcsinh}\left(\frac{1}{2\pi} \right) \sim 0.08 . \tag{2.29}$$

When the singular value has a large hierarchy $\frac{\lambda_{\max}}{\lambda_{\min}} \gg 1$, $R_{\max}(\tau)$ can easily diverge, which is nothing but the hierarchical growth problem.

The ratio $\eta(H) \equiv \frac{\lambda_{\max}}{\lambda_{\min}}$ represents the condition number of the matrix H. Let us evaluate this quantity explicitly in the case of a harmonic oscillator using (2.15). For $mT < \pi$, all
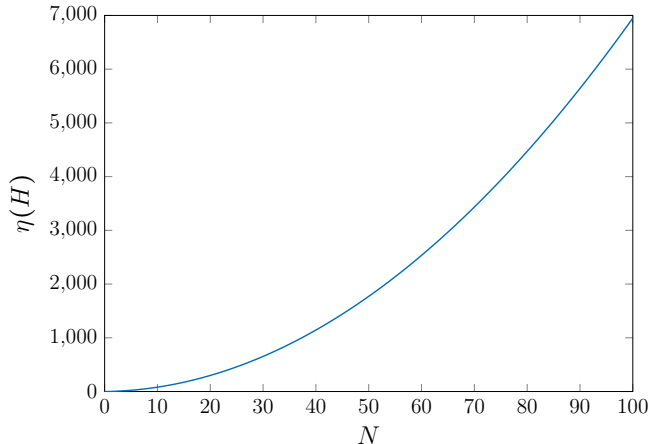
9

Figure 1: The condition number $\eta(H)$ given by (2.30) in the case of a harmonic oscillator is plotted against N for $m^2 = 1$ and $T = 2$, which shows quadratic growth at large N.

the eigenvalues become positive $\tilde{\lambda}_j > 0$ for sufficiently large N. In that case, $\eta(H)$ can be easily evaluated as

$$\eta(H) = \frac{4(N+1)^2 \sin^2 \frac{N\pi}{2(N+1)} - (mT)^2}{4(N+1)^2 \sin^2 \frac{\pi}{2(N+1)} - (mT)^2} \tag{2.30}$$

$$\sim \frac{4}{\pi^2 - (mT)^2} N^2 , \tag{2.31}$$

in the $N \to \infty$ limit with fixed m^2 and T, which corresponds to the continuum limit. In Fig. 1, we plot $\eta(H)$ against N for $m^2 = 1$ and $T = 2$. By plugging these values in (2.28), one finds that R_{max} is as large as 2.4×10^9 even for $N = 20$ used in our numerical simulation in Section 4.4.

Let us also note that the Jacobian that appears in (2.23) has a modulus that can be written in terms of the magnification factor $R_j(\sigma)$ defined in (2.21) as

$$|\det J| = \prod_{j=1}^{N} R_j(\tau) \sim e^{\Lambda \tau} , \tag{2.32}$$

where $\Lambda = \sum_{j=1}^{N} \lambda_j$ grows quadratically with N in the continuum limit. In the present example of a harmonic oscillator, the Jacobian is a constant that does not depend on the variables y_j, which simply factors out of the integral in (2.23) as we already mentioned. This is not the case in a general system, however. The Jacobian with a huge modulus depending on the configuration can cause an overlap problem in the on-axis approach as we discussed in the Introduction.

In the example discussed above, the origin of the large $\eta(H)$ is the ratio of the momenta in the UV and IR regions as one can see from (2.30). This is closely related to the recent discussion that the flow equation in the continuum theory does not allow a well-behaved solution due to the high frequency modes [35]. In order to solve this problem, it was proposed to modify the real part of the action that appears on the right-hand side of the flow equation in the vicinity of the saddle points.

As we have seen in Section 2.1, a similar problem occurs generally in a discretized theory with a large number N of variables, which typically exhibits a large hierarchy in the singular value spectrum of the Hessian. We solve this problem by modifying the flow equation so that the growth rate of each mode becomes identical, while keeping the crucial property of the flow intact.

3 A solution to the hierarchical growth problem

Our basic strategy to solve the hierarchical growth problem is to normalize the growth rates at each step of the flow. For instance, in the example of a harmonic oscillator discussed in the previous section, we can replace (2.18) by

$$\frac{\partial z_j(y,\sigma)}{\partial \sigma} = i \, \frac{\tilde{\lambda}_j}{|\tilde{\lambda}_j|} \, \overline{z_j(y,\sigma)} \; , \tag{3.1}$$

without spoiling the crucial property (2.4) of the flow equation. Thus the hierarchical growth problem can be completely solved. What we aim to do here is to generalize this prescription to an arbitrary system.

3.1 Preconditioned gradient flow equation

Let us first note that the crucial property (2.4) of the gradient flow equation holds for more general flows described by[10]

$$\frac{dz_j}{d\sigma} = \mathcal{A}_{jk}(z,\bar{z}) \, \overline{\frac{\partial S}{\partial z_k}} \; , \tag{3.2}$$

with $\mathcal{A}(z,\bar{z})$ being an arbitrary positive-definite hermitian matrix, which is not necessarily a holomorphic function of z. This can be proved easily as

$$\frac{dS(z(\sigma))}{d\sigma} = \frac{\partial S}{\partial z_j} \mathcal{A}_{jk}(z,\bar{z}) \overline{\frac{\partial S}{\partial z_k}} > 0 \; . \tag{3.3}$$

---

[10]Recently, it has been found that introducing a kernel in the complex Langevin equation is useful in stabilizing simulations in the CLM for real-time quantum evolution [36, 37, 38].

Note that $\mathcal{A}$ changes not only the deformed contour Σ_τ but also the thimbles Σ_∞. However, since the crucial property of the flow is kept intact, Im S is constant on each thimble, which implies that the sign problem can be solved in the same way. We discuss this point in Appendix B with an explicit example.

For the generalized flow (3.2), we find that the displacement $\zeta(\sigma) \equiv z(x+\delta x, \sigma) - z(x, \sigma)$ of the two points after some flow time σ is given by the equation

$$\frac{d}{d\sigma}\zeta_i(\sigma) = \mathcal{A}_{ik}\overline{H_{kl}(z(\sigma))\,\zeta_l(\sigma)} + \left(\frac{\partial \mathcal{A}_{il}}{\partial z_k}\zeta_k(\sigma) + \frac{\partial \mathcal{A}_{il}}{\partial \bar{z}_k}\overline{\zeta_k(\sigma)}\right)\overline{\frac{\partial S(z(\sigma))}{\partial z_l}}\,, \qquad (3.4)$$

instead of the original one (2.5). Let us here assume that the first term is dominant[11] in (3.4). Then the solution to (3.4) can be written formally as (2.9) with $\mathcal{H}(\sigma)$ replaced by[12]

$$\widetilde{\mathcal{H}}(\sigma) = \begin{pmatrix} & \mathcal{A}\,\overline{H(z(\sigma))} \\ \bar{\mathcal{A}}\,H(z(\sigma)) & \end{pmatrix}\,. \qquad (3.5)$$

Recalling the singular decomposition (2.10) of $H(z(\sigma))$, we can choose

$$\mathcal{A} = U(\sigma)^\dagger\,\Lambda^{-1}(\sigma)\,U(\sigma)\,, \qquad (3.6)$$

so that the problematic hierarchy of singular values in $H(z(\sigma))$ is completely eliminated as

$$\bar{\mathcal{A}}\,H(z(\sigma)) = U^\top(\sigma)\,U(\sigma)\,. \qquad (3.7)$$

In this case, the $2N \times 2N$ matrix $\widetilde{\mathcal{H}}(\sigma)$ is again Hermitian and it has N eigenvalues of 1 and -1, respectively; namely the growth rate of each eigenmode becomes identical. (See (2.11).) From this point of view, (3.6) can be regarded as the optimal choice for the "preconditioner" $\mathcal{A}$ in the generalized flow equation (3.2).

In order to implement this idea in practice, let us note that (3.6) can be written as[13]

$$\mathcal{A}(z(\sigma), \overline{z(\sigma)}) = \left\{H^\dagger(z(\sigma))H(z(\sigma))\right\}^{-1/2} = \left\{\overline{H(z(\sigma))}H(z(\sigma))\right\}^{-1/2}\,. \qquad (3.8)$$

Here we use the rational approximation

$$x^{-1/2} \approx a_0 + \sum_{q=1}^{Q}\frac{a_q}{x + b_q}\,, \qquad (3.9)$$

---

[11]This assumption is valid when $z(\sigma)$ is close to a saddle point, for instance. Otherwise, it should be simply regarded as a working hypothesis.

[12]Note that $\widetilde{\mathcal{H}}(\sigma)$ is not Hermitian in general unlike $\mathcal{H}(\sigma)$.

[13]When H has zero singular values, the preconditioner $\mathcal{A}$ has to be regularized, for instance, as $\mathcal{A} = (\bar{H}(\bar{z})H(z) + \varepsilon)^{-1/2}$ with a small positive ε. This is needed when one treats a system with symmetries. While the deformed contour changes with ε, the integral remains unaltered.

which can be made accurate for a wide range of $x > 0$ with the real positive parameters a_q and b_q generated by the Remez algorithm. Thus we obtain

$$\mathcal{A}(z, \bar{z}) \approx a_0 \, \mathbf{1}_N + \sum_{q=1}^{Q} a_q \left\{ \overline{H(z)} H(z) + b_q \, \mathbf{1}_N \right\}^{-1} . \tag{3.10}$$

The matrix inverse $(\bar{H}H + b_q \mathbf{1}_N)^{-1}$ does not have to be calculated explicitly since it only appears in the algorithm as a matrix that acts on some vector, which allows us to use an iterative method for solving a linear equation such as the conjugate gradient (CG) method. The factor of Q in the computational cost can be avoided by the use of a multi-mass CG solver [39, 40]. These techniques are well known in the so-called Rational HMC algorithm [41, 42], which is widely used in QCD with dynamical strange quarks [43] and supersymmetric theories such as the BFSS and IKKT matrix models (See Refs. [44, 45, 46], for example.).

3.2 Calculation of the Jacobian

In the GTM, one has to calculate the Jacobian associated with the change of variables defined by the gradient flow. In the on-thimble approach, only the phase factor of the Jacobian has to be reweighted, while in the on-axis approach, not only the phase factor but also the modulus has to be reweighted. The calculation of the Jacobian gets modified when one introduces the preconditioner to the flow equation. In this subsection, we discuss how this can be done efficiently.

Let us note first that the flow of the Jacobi matrix is given by[14]

$$\frac{d}{d\sigma} J_{ij}(\sigma) = \mathcal{A}_{ik} \overline{H_{kl}(z(\sigma)) \, J_{lj}(\sigma)} + \left(\frac{\partial \mathcal{A}_{il}}{\partial z_k} J_{kj}(\sigma) + \frac{\partial \mathcal{A}_{il}}{\partial \bar{z}_k} \overline{J_{kj}(\sigma)} \right) \overline{\frac{\partial S(z(\sigma))}{\partial z_l}} , \tag{3.11}$$

for the preconditioned flow equation (3.2). (The corresponding flow for the original flow equation (2.2) can be retrieved by setting $\mathcal{A}$ to an identity matrix.) Using the expression (3.10), the derivative of $\mathcal{A}$ in (3.11) can be calculated as

$$\frac{\partial \mathcal{A}}{\partial z_k} = -\sum_{q=1}^{Q} a_q (\bar{H}H + b_q \mathbf{1}_N)^{-1} \bar{H} \frac{\partial H}{\partial z_k} (\bar{H}H + b_q \mathbf{1}_N)^{-1} ,$$

$$\frac{\partial \mathcal{A}}{\partial \bar{z}_k} = -\sum_{q=1}^{Q} a_q (\bar{H}H + b_q \mathbf{1}_N)^{-1} \overline{\frac{\partial H}{\partial z_k}} H (\bar{H}H + b_q \mathbf{1}_N)^{-1} . \tag{3.12}$$

---

[14]The flow equation (3.4) for the displacement can be obtained from (3.11) by using $\zeta_j(\sigma) = J_{jk}(\sigma) \, \delta x_k$.

Note that the matrix inverse $(\bar{H}H + b_q\mathbf{1}_N)^{-1}$ appears twice in the above expressions. In order to use the idea of the multi-mass solver, which enables us to avoid repeating the CG procedure Q times (See the explanation below Eq. (3.10).), we have to apply the matrix inverse to some different vectors separately. For that, we regard the matrix equation (3.11) as a set of vector equations for $i = 1, \cdots, N$. We can calculate the right-hand side of the vector equation for a particular $i = I$ by multiplying a unit vector $e_i^{(I)} = \delta_{iI}$ to the right-hand side of (3.11). Thus the matrix inverse $(\bar{H}H + b_q\mathbf{1})^{-1}$ that appears in (3.12) can be applied to the two vectors $e_i^{(I)}$ and $\overline{\partial_l S}$ separately.

In fact, the expressions (3.12) have to be used also when we compute the force term in the HMC algorithm in the on-axis approach. (See Appendix C for a brief review.) In that case, too, we can apply the idea of the multi-mass solver thanks to the structure of calculations in the backpropagation as we discuss in Appendix D.

The calculation of the Jacobi matrix that we discussed above requires $\mathrm{O}(N^2)$ computational cost for a local action since it involves multiplications of a sparse matrix to a dense matrix[15]. On the other hand, the calculation of its determinant requires $\mathrm{O}(N^3)$ computational cost, which is not affected by the preconditioning at all. These calculations appear only in the reweighting procedure, which can be done off-line after generating configurations, and the procedure can be parallelized trivially without any overhead due to communications. On the other hand, all the calculations for generating configurations require only $\mathrm{O}(N)$ computational cost for a local action even after implementing the preconditioner in the gradient flow equation since it just involves multiplications of a sparse matrix to a vector.

In passing, let us also mention that there is actually a cheaper preconditioner, which can be obtained by considering only the free part of the action when we calculate the Hessian H to be used in (3.8). Since the preconditioner $\mathcal{A}(z, \bar{z})$ in this case becomes a constant matrix independent of the configuration, we only have to compute $\mathcal{A}$ and diagonalize it once and for all. The rational approximation (3.10) is not needed any more. This cheaper preconditioner works efficiently in the weak coupling regime, and the computational cost can be reduced typically by an order of magnitude compared to the full preconditioner.

4 Demonstration of the preconditioned flow

In this section, we demonstrate how the preconditioned flow equation works in the application of GTM to the real-time quantum evolution of an anharmonic oscillator. Here we

---

[15]For a non-local action, the cost increases by a factor of $\mathrm{O}(N)$ since the sparseness is lost.

use the on-axis approach for the HMC algorithm, where the force term is calculated by the backpropagation [26]. In particular, we show that the long autocorrelation in the generated configurations is drastically reduced by preconditioning the flow. We also show that the preconditioning drastically reduces the modulus of the Jacobian and its fluctuations, thereby solving the overlap problem in the on-axis approach.

4.1 Simulation setup

The system we deal with in this section is the same as (2.13) except that we consider an anharmonic potential

$$V(x) = \frac{1}{4!} \lambda x^4 \ . \tag{4.1}$$

Here we introduce the initial wave function

$$\psi_i(x) \propto \exp \left\{ -\frac{1}{4} \gamma \, (x - x_i)^2 \right\} \ , \tag{4.2}$$

and calculate the time-evolved wave function $\psi_f(x)$ after some time T, which is given by the path integral (2.1) up to some known normalization factor using the action

$$S(x; x_f, x_i) = -i \sum_{j=1}^{N} \epsilon \left\{ \frac{1}{2} \left(\frac{x_{j+1} - x_j}{\epsilon} \right)^2 - \frac{V(x_{j+1}) + V(x_j)}{2} \right\} + \frac{1}{4} \gamma \, (x_1 - x_i)^2 \ , \tag{4.3}$$

where $T = N\epsilon$ and $x_{N+1} \equiv x_f$. Similar calculations have been done using the original flow in Ref. [26] although N had to be restricted to small values such as $N = 9$. The main point here is that the preconditioned flow enables us to increase N without any problems.

In order to avoid the ergodicity problem concerning multiple thimbles, we integrate over the flow time [24] as described in Ref. [26] in the on-axis approach. The Hamiltonian to be used in the fictitious Hamilton dynamics of the HMC algorithm is given by

$$H = \frac{1}{2m^2(\tau)} \sum_{j=1}^{N} p_j^2 + \frac{1}{2\tilde{m}^2} p_\tau^2 + \mathrm{Re} \, S(z(x, \tau)) + W(\tau) \ , \tag{4.4}$$

where p_j and p_τ are the conjugate momenta corresponding to x_j and the flow time τ, respectively. The function $m(\tau)$ and the parameter $\tilde{m}$ are introduced for optimization as we explain shortly. The total time s_f and the step size Δs for the fictitious Hamilton dynamics are the parameters of the HMC algorithm that can be optimized in a standard manner. In all our simulations, we choose $s_f = 1$ and $\Delta s = 0.05$, and the number of time steps for solving the flow equation is set to $N_\tau = 10$.
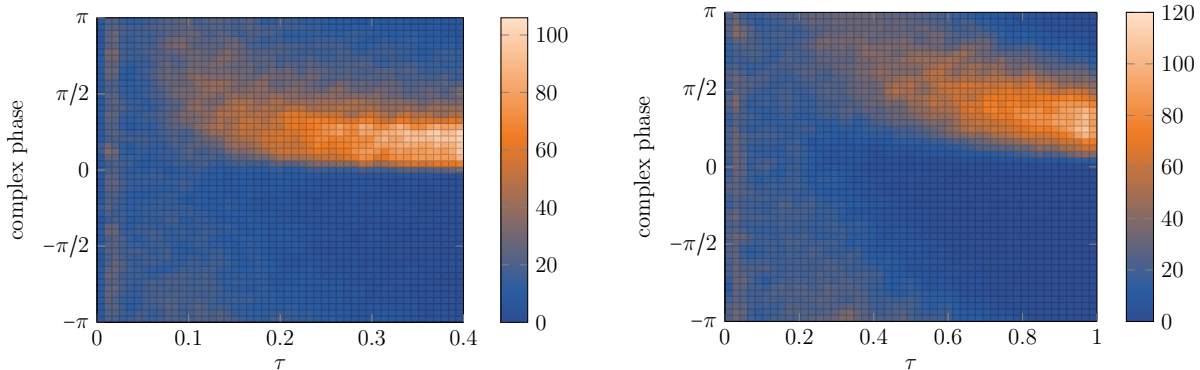
Figure 2: The distribution of the phase of the integrand of (2.3) and the flow time τ obtained by simulations is shown for the original flow (Left) and the preconditioned flow (Right) in the case of $N = 6$, $T = 2$, $\lambda = 1$, $x_{\mathrm{i}} = 1$, $\gamma = 1$ and $x_{\mathrm{f}} = 0$. The color indicates the number of configurations in each bin. The total number of configurations is 50000, and we have 50 bins in both the horizontal and vertical directions.

The parameter $\tilde{m} > 1$ in (4.4) is introduced only for simulations with the original flow in order to avoid the force in the τ-direction getting too large depending on x, which causes the drop of the acceptance rate. We have increased $\tilde{m}$ from unity until the acceptance rate becomes reasonably high.

On the other hand, the function $m(\tau)$ in (4.4) is chosen to be the typical largest singular value of the Jacobi matrix $J(x, \tau)$ based on the discussion in Section 2 so that the eigenmode with the largest growth rate does not diverge.[16] Then the hierarchical growth problem manifests itself as long autocorrelation due to the modes with small growth rate.

The function $W(\tau)$ in (4.4) is determined so that the distribution of τ becomes flat within the region $\tau \in [\tau_{\min}, \tau_{\max}]$, where $\tau_{\max}$ has to be chosen to be large enough to solve the sign problem and $\tau_{\min}$ has to be chosen to be small enough to solve the ergodicity problem. The actual form of the function $W(\tau)$ as well as that of $m(\tau)$ is determined iteratively by improving them step by step using the results obtained by the previous simulation.

Let us discuss how we determine the optimal region $[\tau_{\min}, \tau_{\max}]$ of τ to be used in the simulation, which actually depends on whether we use the preconditioned flow or not. In Fig. 2, we show the distribution of the phase of the integrand in (2.3) including the phase coming from the Jacobian for the original flow (Left) and the preconditioned flow (Right) in the case of $N = 6$, $T = 2$, $\lambda = 1$, $x_{\mathrm{i}} = 1$, $\gamma = 1$ and $x_{\mathrm{f}} = 0$.

---

[16]In Ref. [26], $m(\tau)$ was chosen to be the typical value of $|\det J(x, \tau)|^{\frac{1}{N}}$, which corresponds to taking the geometric average of the growth rate. However, the effective stepsize in this case becomes too large for the eigenmode with the largest growth rate, which causes divergence during simulations at large N.
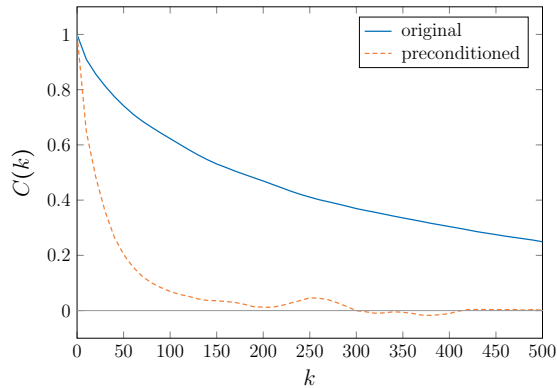
Figure 3: The autocorrelation of $\mathbf{x}$ is plotted against the number of separation using 50000 configurations obtained by simulations with $N = 6$, $T = 2$, $\lambda = 1$, $x_{\mathrm{i}} = 1$, $\gamma = 1$ and $x_{\mathrm{f}} = 0$. The blue solid line and the orange dashed line represent the results obtained by the original flow and the preconditioned flow, respectively.

The sign problem is solved in the region of τ that exhibits some non-uniformity in the distribution of the phase. However, in order to avoid the ergodicity problem, one should also sample the region of τ in which the distribution of the phase is almost uniform. Based on these criteria, we choose the range of τ to be $[0.02, 0.2]$ for the original flow, and $[0.4, 0.8]$ for the preconditioned flow in this case.

See Appendix E for the choice of the parameters $\tilde{m}$, $\tau_{\min}$, $\tau_{\max}$, $m(\tau)$ and $W(\tau)$ determined in the way described above for each case.

4.2 Reduction of the autocorrelation

Let us first show that the autocorrelation is drastically reduced by preconditioning the flow equation. We define the autocorrelation in the generated configurations $\mathbf{x} = (x_1, \cdots, x_N)$ as follows. Let $\mathbf{x}^{(k)}$ $(k = 1, \cdots, n)$ be the k-th configuration. We denote the average of the n configurations as $\overline{\mathbf{x}} = \frac{1}{n} \sum_{k=1}^{n} \mathbf{x}^{(k)}$. Then the autocorrelation can be defined as

$$C(k) \equiv \frac{1}{v} \frac{1}{n-k} \sum_{m=1}^{n-k} (\mathbf{x}^{(m)} - \overline{\mathbf{x}}) \cdot (\mathbf{x}^{(m+k)} - \overline{\mathbf{x}}) \,, \tag{4.5}$$

where v is the variance defined by

$$v = \overline{\mathbf{x} \cdot \mathbf{x}} - \overline{\mathbf{x}} \cdot \overline{\mathbf{x}} \,. \tag{4.6}$$

In Fig. 3, we show the autocorrelation of $\mathbf{x} = (x_j)$ obtained by simulations with the same parameters as in Fig. 2. The region of τ is chosen to be $[0.02, 0.2]$ and $[0.4, 0.8]$ for the
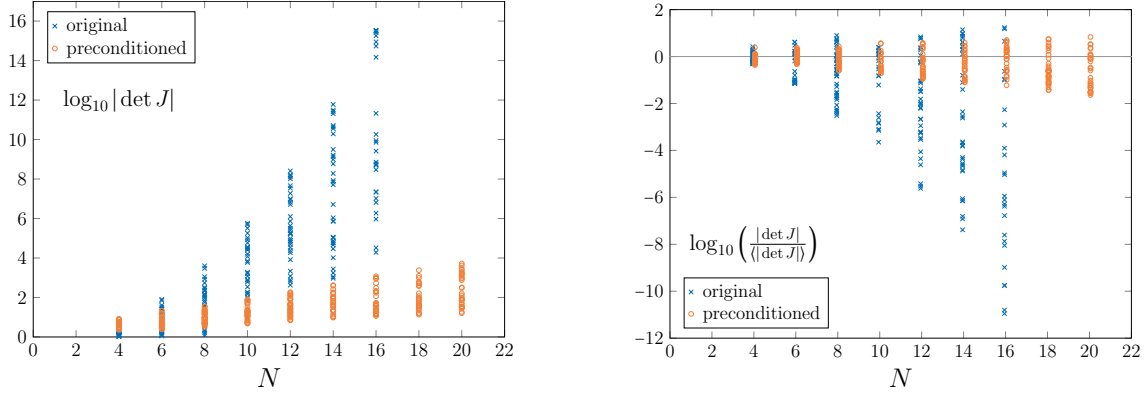
17

Figure 4: (Left) The scattered plots of the modulus $|\det J|$ of the Jacobian obtained by simulations is shown for various N ($4 \leq N \leq 20$) in the case of $T = 2$, $\lambda = 1$, $x_{\mathrm{i}} = 1$, $\gamma = 1$ and $x_{\mathrm{f}} = 0$. The blue crosses and the orange circles represent the results for the original flow and the preconditioned flow, respectively. For each N, we have used 30 configurations obtained within 10000 trajectories. (Right) Similar plots for the normalized modulus $|\det J|/\langle|\det J|\rangle$ of the Jacobian are shown for various N.

original flow and the preconditioned flow, respectively. We find that the autocorrelation is reduced by a factor of 10 for the preconditioned flow, which suggests that the hierarchical growth problem is avoided.

4.3 Reduction of the modulus of the Jacobian

Next we discuss the Jacobian associated with the change of variables by the gradient flow, which can typically have a large modulus as we mentioned below (2.32) in Section 2.2. This, in particular, causes the overlap problem in the on-axis approach. We will see below that the preconditioned flow reduces the modulus of the Jacobian and its fluctuation drastically, thereby solving this problem as well as the hierarchical growth problem.

In Fig. 4 (Left), we show the scattered plot of $\log_{10}|\det J|$ obtained by simulations for various N ($4 \leq N \leq 20$) with $T = 2$, $\lambda = 1$, $x_{\mathrm{i}} = 1$, $\gamma = 1$ and $x_{\mathrm{f}} = 0$. We have fixed the range of τ as $[0.02, 0.2]$ and $[0.4, 0.8]$ for the cases with and without preconditioning, respectively. The blue crosses and the orange circles represent the results for the original flow and the preconditioned flow, respectively. Our results show that the preconditioning reduces the values of $|\det J|$ drastically as expected. Furthermore, from Fig. 4 (Right), we find that the preconditioning suppresses the fluctuation of $|\det J|$ drastically, which suggests that it can also solve the overlap problem in the on-axis approach.

Without preconditioning, it was not even possible to perform simulations for $N > 16$
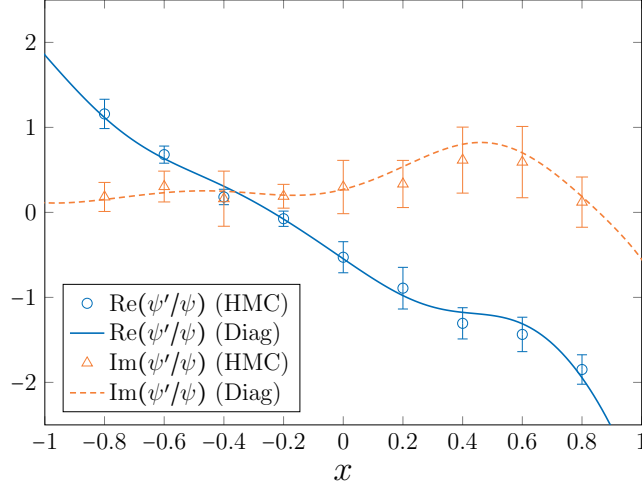
Figure 5: The quantity (4.7) derived from the time-evolved wave function is shown for $N = 20$, $T = 2$, $\lambda = 30$, $x_{\mathrm{i}} = 0.3$ and $\gamma = 4$. The blue circles and the orange triangles represent the real part and the imaginary part, respectively. Each point is obtained by taking an average over 30000 configurations generated by an independent simulation using $x_{\mathrm{f}} = x$. The blue solid line (real part) and the orange dashed line (imaginary part) represent the results obtained by solving the Schrödinger equation with Hamiltonian diagonalization.

since the typical magnitude of the HMC force in the τ-direction changes too much with x, and we were not able to control it by the x-independent potential $W(\tau)$. This may be viewed as another manifestation of the hierarchical growth problem. Such behaviors were not seen in simulations with the preconditioned flow.

4.4   Result for the time-evolved wave function

Finally we show that the preconditioned flow enables us to obtain results for the time-evolved wave function $\psi_{\mathrm{f}}(x_{\mathrm{f}})$ even at large N and at strong coupling (large λ). As has been done in Ref. [26], we calculate

$$\frac{\partial}{\partial x_{\mathrm{f}}} \log(\psi_f(x_{\mathrm{f}})) = -\left\langle \frac{\partial S}{\partial x_{\mathrm{f}}} \right\rangle = \left\langle i \left(\frac{x_{\mathrm{f}} - x_N}{\epsilon} - \frac{\epsilon}{2} V'(x_{\mathrm{f}}) \right) \right\rangle , \qquad (4.7)$$

which is directly accessible by calculating the expectation value on the right-hand side. In Fig. 5, we show our results for $N = 20$, $T = 2$, $\lambda = 30$, $x_{\mathrm{i}} = 0.3$ and $\gamma = 4$. For each x_{f}, we have determined the range of τ as presented in Appendix E. Our results are in good agreement with the results obtained by solving the Schrödinger equation with Hamiltonian diagonalization.

In Ref. [26], it was difficult to obtain reliable results as one goes beyond $N = 9$ because of the overlap problem even at $\lambda = 1$. Here we are able to obtain results for $N = 20$ even at strong coupling $\lambda = 30$ without any problems.

5   Summary and discussions

In this paper we have pointed out a problem in the gradient flow equation, which is used in the GTM to deform the integration contour into the complex plane. The property of the flow that plays an important role in solving the sign problem is that it maps a small region on the real axis to a region on the deformed contour which becomes exponentially large with the flow time. The problem is that the growth rate for each mode typically has a huge hierarchy when the system size becomes large. If one chooses the flow time to be large enough to solve the sign problem associated with the slowly growing modes, the fast growing modes tend to diverge.

In order to solve this hierarchical growth problem, we have proposed to modify the flow equation by the preconditioner, which makes the growth rate equal without spoiling the crucial properties of the flow equation. This preconditioner can be implemented practically in the GTM with the standard techniques used in the Rational HMC algorithm.

We applied this method to the real-time quantum evolution of an anharmonic oscillator using the on-axis approach with backpropagation for calculating the HMC force [26]. In the on-axis approach, the hierarchical growth problem manifests itself in the long auto-correlation time since one cannot choose the parameters in the HMC algorithm for each mode separately. Our results indeed show that the auto-correlation time is reduced drastically. Moreover, the modulus of the Jacobian, which has to be taken into account by reweighting, is also reduced drastically. This solves the overlap problem in reweighting, which is caused by large fluctuations of the modulus of the Jacobian. Thus we were able to simulate the system with the size N that was not accessible without preconditioning the flow [26]. Note also that this is achieved with a very strong coupling $\lambda = 30$ in the quartic potential (4.1), which makes the flow equation highly non-linear.

As a side remark, the preconditioned flow solves yet another problem of the original gradient flow, which occurs when the integrand has zeroes [27]. In that case, there are points on the real axis that flow into the zeroes within finite flow time, and the right-hand side of the flow equation blows up as one approaches the zeroes. A practical solution proposed in Ref. [27] is to add some regulator to the flow equation, which modifies the flow only in the vicinity of the zeroes. We consider that this problem does not occur for the preconditioned flow since the preconditioner cancels the divergence of the right-hand side

that occurs as one approaches the zeroes. See Appendix A for discussions on this issue.

While we focused on the on-axis approach in this paper, the hierarchical growth problem of the flow may also affect the on-thimble approach. There, we have to solve a set of equations iteratively by Newton's method in order to make sure that the updated configurations are constrained on the deformed contour. This procedure appears at every step of the fictitious time evolution in the HMC algorithm. The coefficient matrix of these equations involves the Jacobian, which has a huge condition number for the original flow. Therefore, the solution of the equations may suffer from large numerical errors and/or slow convergence when the system size becomes large. The preconditioned flow may be useful in solving such problems. (See Ref. [47] for a new proposal related to this issue.)

As we have shown in this paper, the preconditioned flow enables us to apply the GTM to much larger systems than those accessible with the original flow. In particular, it gives us an access to the continuum limit and to the strong coupling regime, which enabled us to establish a new picture of quantum tunneling in the real-time path integral formalism [33]. We expect that there are many other applications awaiting us to explore.

Acknowledgements

A   The absence of the blow-up problem

Here we discuss a problem that occurs when the integrand of the partition function has zeroes. In such a case, the gradient flow can reach the zeroes within finite flow time and the right-hand side of the flow equation blows up. This is the blow-up problem of the GTM, which was discussed in Ref. [27]. Let us first emphasize that this problem occurs although the partition function is totally well defined. The deformed contour one obtains at sufficiently long flow time is nothing but a set of contours connected at the zeroes[17] . It is therefore just a technical problem of how to deal with the divergence that occurs while

---

[17]See Ref. [48] for recent discussions on this case.

solving the flow equation. Here we argue that this problem is naturally avoided in the preconditioned flow since it slows down the flow as one approaches the zeroes.

To simplify the argument, we consider a single-variable case $N = 1$ in (2.1) with real $S(x)$. In this case, the original flow equation (2.2) reads

$$\frac{dx(\sigma)}{d\sigma} = S'(x(\sigma)) , \tag{A.1}$$

whereas the preconditioned flow (3.2) with (3.8) reads

$$\frac{dx(\sigma)}{d\sigma} = \frac{S'(x(\sigma))}{|S''(x(\sigma))|} , \tag{A.2}$$

where $'$ represents the derivative with respect to x.

For instance, let us consider the case with

$$S(x) = \frac{1}{2(n+1)} x^{2(n+1)} , \qquad n = 1, 2, \cdots , \tag{A.3}$$

which gives $e^{-S(x)} \to 0$ for $x \to \pm\infty$. The saddle point is $x = 0$, and there are flows towards the singularities at $x = \pm\infty$. Solving the original flow equation (A.1), one obtains

$$x(\sigma) = \begin{cases} \{x(0)^{-2n} - 2n\sigma\}^{-\frac{1}{2n}} & \text{for } x(0) > 0 , \\ -\{x(0)^{-2n} - 2n\sigma\}^{-\frac{1}{2n}} & \text{for } x(0) < 0 , \end{cases} \tag{A.4}$$

which reaches the singularities within finite flow time $\sigma = \frac{1}{2n}x(0)^{-2n}$. However, for the preconditioned flow (A.2), one obtains

$$x(\sigma) = x(0) \, e^{\sigma/(2n+1)} , \tag{A.5}$$

which reaches the singularities only in the $\sigma \to \infty$ limit.

Next we consider the case with[18]

$$S(x) = -\log(x^{2n}) , \qquad n = 1, 2, \cdots , \tag{A.6}$$

which gives $e^{-S(x)} \to 0$ for $x \to 0$. The saddle point is $x = \pm\infty$, and there are flows towards the singularity at $x = 0$. Solving the original flow equation (A.1), one obtains

$$x(\sigma) = \begin{cases} \sqrt{x(0)^2 - 4n\sigma} & \text{for } x(0) > 0 , \\ -\sqrt{x(0)^2 - 4n\sigma} & \text{for } x(0) < 0 , \end{cases} \tag{A.7}$$

---

[18]Strictly speaking, the partition function is not finite in this case. In order to make it finite, one can add a term like $\frac{1}{2}\epsilon x^2$ in the action, which clearly does not affect the flow near the singularity $x = 0$.

which reaches the singularity within finite flow time $\sigma = \frac{1}{4n}x(0)^2$. However, for the preconditioned flow (A.2), one obtains

$$x(\sigma) = x(0)\, e^{-\sigma}\,, \tag{A.8}$$

which reaches the singularity only in the $\sigma \to \infty$ limit.

Thus the preconditioning (A.2) makes the singularities unreachable within finite flow time. While we have discussed a single variable case with a real action for simplicity, this property of the preconditioned flow is considered to be quite general. For instance, the quantum mechanical system with the anharmonic potential (4.1) suffers from a blow-up problem for sufficiently long flow time if one uses the original flow equation similarly to the example (A.3). We consider that the preconditioned flow naturally avoids this problem. A more careful study on this issue shall be left for future investigations.

B Modification of the thimbles by preconditioning

The preconditioning of the gradient flow equation changes the deformed contour. In fact, it also modifies the Lefschetz thimbles, which appear as the deformed contour in the long flow time $\tau \to \infty$ limit. On the other hand, the preconditioning does not alter the saddle points, which are defined by $\frac{\partial S(z)}{\partial z} = 0$ independently of the flow. In this section, we discuss these points using a simple example.

Let us consider an integral (2.1) with $N = 2$ variables, where the action is given by

$$S(z) = \frac{1}{2}(z_1{}^2 - iz_2{}^2)\,. \tag{B.1}$$

The saddle point is given by $z_1 = z_2 = 0$. The original flow equations read

$$\frac{dz_1}{d\sigma} = \bar{z}_1\,, \qquad \frac{\partial z_2}{\partial \sigma} = i\bar{z}_2\,, \tag{B.2}$$

which is linear. Using the real-variable notation $z_1 = x_1 + iy_1$, $z_2 = x_2 + iy_2$, the flow equation (B.2) can be rewritten as

$$\frac{d}{d\sigma}\begin{pmatrix} x_1 \\ y_1 \\ x_2 \\ y_2 \end{pmatrix} = M \begin{pmatrix} x_1 \\ y_1 \\ x_2 \\ y_2 \end{pmatrix}\,, \qquad M = \begin{pmatrix} 1 & & & \\ & -1 & & \\ & & & 1 \\ & & 1 & \end{pmatrix}\,. \tag{B.3}$$

The Lefschetz thimble Σ_∞ is spanned by the eigenvectors of the matrix M corresponding to positive (degenerate) eigenvalue 1, which are given by

$$v_1 = \begin{pmatrix} 1 \\ 0 \\ 0 \\ 0 \end{pmatrix} \,, \qquad v_2 = \begin{pmatrix} 0 \\ 0 \\ 1 \\ 1 \end{pmatrix} \,. \tag{B.4}$$

Next we consider the generalized flow (3.2) with a preconditioner[19]

$$\mathcal{A} = \begin{pmatrix} 5 & 1 \\ 1 & 5 \end{pmatrix} \,. \tag{B.5}$$

The preconditioned flow equations are given by

$$\frac{\partial z_1}{\partial \sigma} = 5\bar{z}_1 + i\bar{z}_2 \,, \qquad \frac{\partial z_2}{\partial \sigma} = \bar{z}_1 + 5i\bar{z}_2 \,. \tag{B.6}$$

Using the real-variable notation, the preconditioned flow equation (B.6) becomes

$$\frac{d}{d\sigma} \begin{pmatrix} x_1 \\ y_1 \\ x_2 \\ y_2 \end{pmatrix} = \widetilde{M} \begin{pmatrix} x_1 \\ y_1 \\ x_2 \\ y_2 \end{pmatrix} \,, \qquad \widetilde{M} = \begin{pmatrix} 5 & & & 1 \\ & -5 & 1 & \\ 1 & & & 5 \\ & -1 & 5 & \end{pmatrix} \,. \tag{B.7}$$

The Lefschetz thimble $\widetilde{\Sigma}_\infty$ is spanned by the eigenvectors of the matrix $\widetilde{M}$ corresponding to positive eigenvalues $4\sqrt{2}$ and $3\sqrt{2}$, which are given, respectively, by

$$\tilde{v}_1 = \begin{pmatrix} 5 + 4\sqrt{2} \\ 5 - 3\sqrt{2} \\ 1 + 5\sqrt{2} \\ 7 \end{pmatrix} \,, \qquad \tilde{v}_2 = \begin{pmatrix} 5 + 3\sqrt{2} \\ 5 - 4\sqrt{2} \\ 1 - 5\sqrt{2} \\ -7 \end{pmatrix} \,. \tag{B.8}$$

Thus we find that the thimble $\widetilde{\Sigma}_\infty$ is different from the original one Σ_∞. Note, however, that both thimbles are embedded in a real 3-dimensional hypersurface defined by $\{(x_1 \ y_1 \ x_2 \ y_2) \mid \operatorname{Im} S = 2x_1 y_1 - x_2^2 + y_2^2 = 0\} \in \mathbb{R}^4$, and therefore the sign problem is solved in both cases.

---

[19]Note that the optimal choice is actually $\mathcal{A} = \mathbf{1}$ in the present case. The aim here is to demonstrate that nontrivial $\mathcal{A}$ modifies the thimble.

C Application of the HMC using the on-axis approach

In this section, we briefly review how one can apply the HMC algorithm to the GTM using the on-axis approach. The key idea that makes this feasible is the backpropagation in calculating the force term in the fictitious Hamilton dynamics of the HMC algorithm [26]. Here we fix the flow time for simplicity, but it is straightforward to implement the integration over the flow time, which is needed in avoiding the ergodicity problem. (See Ref. [26] for the details.)

Let us consider the general partition function given by (2.1). The expectation value of the observable is defined by

$$\langle \mathcal{O} \rangle = \frac{1}{Z} \int_{\mathbb{R}^N} dx \, e^{-S(x)} \mathcal{O}(x) \; . \tag{C.1}$$

In the GTM, this integral is evaluated by

$$\langle \mathcal{O} \rangle = \frac{1}{Z} \int_{\Sigma_\tau} dz \, e^{-S(z)} \mathcal{O}(z) \; , \tag{C.2}$$

where τ is the flow time and the integration contour Σ_τ is defined by solving the gradient flow equation (2.2).

When one applies the HMC algorithm to evaluate this integral, one has to define a fictitious Hamilton dynamics to update the configuration on the deformed contour. In the on-thimble approach, one defines the Hamilton dynamics on Σ_τ, which is a classical mechanics of a constrained system. Since the deformed contour Σ_τ is not given explicitly but has to be determined by solving the flow equation, complicated procedures are necessary in solving the Hamilton equation in such a way that the configuration is always on Σ_τ.

In the on-axis approach, on the other hand, one rewrites the integral (C.2) as

$$\langle \mathcal{O} \rangle = \frac{1}{Z} \int_{\mathbb{R}^N} dx \, \det J(x, \tau) \, e^{-S(z(x))} \mathcal{O}(z(x)) \; , \tag{C.3}$$

and defines the Hamilton dynamics on the real axis $\mathbb{R}^N$. Here $J(x, \tau)$ is the Jacobi matrix associated with the change of variables $x \mapsto z(x, \tau)$, which obeys the following flow equation

$$\frac{\partial}{\partial \sigma} J_{kl}(x, \sigma) = \overline{H_{km}(z(x, \sigma)) J_{ml}(x, \sigma)} \; , \tag{C.4}$$

where H_{km} is the Hessian defined by (2.6).

The fictitious Hamilton dynamics is defined by the Hamiltonian

$$H = \frac{1}{2} \sum_{i=1}^{N} p_i^2 + \operatorname{Re} S(z(x, \tau)) \; , \tag{C.5}$$

where p_i are the momentum variables conjugate to the coordinate variables x_i. Note that there is no constraint that complicates the Hamilton dynamics unlike the on-thimble approach. In order to obtain the expectation value of the observables, one uses the reweighting

$$\langle \mathcal{O} \rangle = \frac{\langle \mathcal{O}(z(x,\tau)) \det J(x,\tau) \, e^{-i \operatorname{Im} S(z(x,\tau))} \rangle_{\text{HMC}}}{\langle \det J(x,\tau) \, e^{-i \operatorname{Im} S(z(x,\tau))} \rangle_{\text{HMC}}} \ , \tag{C.6}$$

where the expectation value $\langle \, \cdot \, \rangle_{\text{HMC}}$ represents an ensemble average over the configurations generated by the HMC algorithm with the Hamiltonian (C.5).

Note that the force term in the Hamilton equation is given by

$$F_j = -\frac{\partial \operatorname{Re} S(x,\tau)}{\partial x_j} = -\operatorname{Re}\left(f_i(x,\tau) J_{ij}(x,\tau) \right) \ , \tag{C.7}$$

$$f_i(x,\tau) = \left. \frac{\partial S(z(x,\tau))}{\partial z_i} \right|_{z=z(x,\tau)} \ . \tag{C.8}$$

If one naively uses this formula to calculate the force term, the Jacobi matrix $J_{ij}(x,\tau)$ that appears in (C.7) requires the computational cost of $O(N^2)$ for a local system since it involves matrix-matrix products. In fact, this can be completely avoided by using the backpropagation [26] as we discuss below.

Let us first note that $z(x,\tau)$ and hence $S(z(x,\tau))$ can be regarded as functions of $z(x,\sigma)$ and $\bar{z}(x,\sigma)$ $(0 \leq \sigma \leq \tau)$ since $z(x,\sigma+\delta\sigma) \simeq z(x,\sigma) + \overline{\partial S(z(x,\sigma))}$. We can therefore define the force at each σ as

$$F_j(\sigma) = \frac{\partial S(z(x,\tau))}{\partial z_j(x,\sigma)} \ , \qquad \bar{F}_j(\sigma) = \frac{\partial S(z(x,\tau))}{\partial \bar{z}_j(x,\sigma)} \ , \tag{C.9}$$

which obeys the relation

$$F_j(\sigma - \delta\sigma) = F_i(\sigma) \frac{\partial z_i(x,\sigma)}{\partial z_j(x,\sigma-\delta\sigma)} + \bar{F}_i(\sigma) \frac{\partial \bar{z}_i(x,\sigma)}{\partial z_j(x,\sigma-\delta\sigma)} \ . \tag{C.10}$$

Thus we can calculate $F_j = F_j(0)$ from $f_j = F_j(\tau)$ by solving (C.10) backward in σ. Note that this is the same procedure as the backpropagation used in machine learning. Since this procedure involves the matrix-vector multiplication only, one can calculate the force term with the computational cost of $O(N)$ for a local system.

D   Backpropagation with the preconditioner

As we have seen in the previous section, backpropagation (C.10) is the key idea that makes the calculation of the force term (C.7) in the HMC algorithm feasible in the on-axis approach. In this section, we discuss how the backpropagation works with the preconditioned gradient flow in a way compatible with the idea of the multi-mass solver.

In the case of the preconditioned flow (3.2), the explicit form of (C.10) is given by

$$F_j(\sigma - \delta\sigma) = F_j(\sigma) + \delta\sigma\, G_j(\sigma) \;, \tag{D.1}$$

$$G_j(\sigma) = F_i(\sigma)(\partial_j \mathcal{A}_{ik})\overline{\partial_k S} + \bar{F}_i(\sigma)\left[\bar{\mathcal{A}}_{ik} H_{kj} + (\partial_j \bar{\mathcal{A}}_{ik})\partial_k S\right] \;. \tag{D.2}$$

By using the rational approximation (3.10) for $\mathcal{A}$, we can rewrite $G_i(\sigma)$ in (D.2) as

$$G_j(\sigma) = -\sum_{q=1}^{Q} a_q \left(F^\top(\sigma)(\bar{H}H + b_q \mathbf{1})^{-1}\bar{H}\right)_i (\partial_j H_{ik})\left((\bar{H}H + b_q \mathbf{1})^{-1}\overline{\partial S}\right)_k + (\bar{F}^\top \bar{\mathcal{A}}H)_j$$

$$-\sum_{q=1}^{Q} a_q \left(\bar{F}^\top(\sigma)(\bar{H}H + b_q \mathbf{1})^{-1}\right)_i (\partial_j H_{ik})\left(\bar{H}(\bar{H}H + b_q \mathbf{1})^{-1}\partial S\right)_k \;. \tag{D.3}$$

As in the calculation of the Jacobian using (3.12), the matrix inverse $(\bar{H}H + b_q \mathbf{1})^{-1}$ in the first line can be applied to the two vectors $F_j(\sigma)$ and $\overline{\partial_j S}$ separately, and similarly for the matrix inverse in the second line. Therefore we can avoid the computational cost of O(Q) by using the idea of the multi-mass solver.

As we discussed in Section 4.1, in order to avoid the ergodicity problem in the GTM, we have to integrate over the flow time, which implies that we have to treat τ as a dynamical variable in the simulation. In the HMC algorithm, we therefore have to calculate the force term for τ as described in Section 4 of Ref. [26]. Below we discuss how this can be done efficiently even in the presence of the preconditioner in the gradient flow.

Since the flow time is discretized as $\tau = N_\tau \delta\tau$ when we solve the gradient flow equation, the derivative with respect to τ used in defining the force $F_\tau(x, \tau)$ for τ is replaced by the derivative with respect to the spacing $\delta\tau$. The force $F_\tau(x, \tau)$ for τ is defined by

$$F_\tau(x, \tau) = \mathrm{Re}\Big(\partial_j S(x, \tau = N_\tau \delta\tau)\, \dot{z}_j(x, \tau = N_\tau \delta\tau)\Big) \;, \tag{D.4}$$

where $\dot{z}_j(x, \tau = N_\tau \delta\tau)$ is defined by the difference equation

$$(n+1)\, \dot{z}_j(x, (n+1)\, \delta\tau)$$
$$= n\, \dot{z}_j(z, n\, \delta\tau) + \mathcal{A}_{jk}\overline{\partial_k S}$$
$$+ n\, \delta\tau\left[\mathcal{A}_{jk}\, \bar{H}_{ki}\, \dot{z}_i(x, n\delta\tau) + (\partial_i \mathcal{A}_{jk})\, \overline{\partial_k S}\, z_i(x, n\delta\tau) + (\bar{\partial}_i \mathcal{A}_{jk})\, \overline{\partial_k S}\, \bar{z}_i(x, n\delta\tau)\right] \tag{D.5}$$

with the condition $\dot{z}_j(z, 0) = 0$. Note that the second term on the right-hand side is an inhomogeneous term, which does not appear in the flow equation (3.11) for the Jacobi matrix. Nevertheless, we can calculate (D.4) by backpropagation as follows.

Using a 2N-dimensional complex vector $\zeta^{(n)} = (\dot{z}(x, n\delta\tau), \dot{\bar{z}}(x, n\delta\tau))^\top$, (D.5) can be written formally as

$$\zeta^{(n+1)} = \mathcal{B}^{(n)}\zeta^{(n)} + \beta^{(n)} \;, \tag{D.6}$$

where $\mathcal{B}^{(n)}$ and $\beta^{(n)}$ are a $2N \times 2N$ matrix and a $2N$-dimensional vector, respectively, both depending on $\zeta^{(n)}$. Then, the force (D.4) for the flow time can be expanded as

$$
\begin{aligned}
2F_\tau &= V^{(N_\tau)\top}\zeta^{(N_\tau)} \\
&= V^{(N_\tau)\top}(\mathcal{B}^{(N_\tau-1)}\zeta^{(N_\tau-1)} + \beta^{(N_\tau-1)}) \\
&= V^{(N_\tau)\top}\mathcal{B}^{(N_\tau-1)}(\mathcal{B}^{(N_\tau-2)}\zeta^{(N_\tau-2)} + \beta^{(N_\tau-2)}) + V^{(N_\tau)\top}\beta^{(N_\tau-1)} \\
&= V^{(N_\tau)\top}\sum_{n=1}^{N_\tau}\left(\prod_{m=0}^{n-1}\mathcal{B}^{(m)}\right)\beta^{(N_\tau-n)} \ ,
\end{aligned}
\tag{D.7}
$$

where we have introduced a $2N$-dimensional vector $V^{(N_\tau)} = (v^{(N_\tau)}, \bar{v}^{(N_\tau)})^\top$ with $v_j^{(N_\tau)} = \partial_j S(x, N_\tau \delta\tau)$ and used the initial condition $\zeta^{(0)} = 0$. The product $\prod_{m=0}^{n-1}$ in the last line should be understood as the time-ordered product, in which $\mathcal{B}^{(m)}$ with smaller m appears on the right. Here we define a vector $V^{(n)\top} \equiv V^{(N_\tau)\top}\mathcal{B}^{(N_\tau-1)}\cdots\mathcal{B}^{(n)}$, which can be obtained recursively by using the relation

$$
V^{(n-1)\top} = V^{(n)\top}\mathcal{B}^{(n-1)} \ .
\tag{D.8}
$$

Then we can obtain the force (D.7) by

$$
2F_\tau = \sum_{j=0}^{N_\tau-1} V^{(j+1)\top}\beta^{(j)} \ .
\tag{D.9}
$$

More explicitly, the algorithm to calculate the force for τ can be derived as follows. Let us represent $V^{(n)}$ as $V^{(n)} = (v^{(n)}, \bar{v}^{(n)})^\top$. From (D.8), we obtain

$$
v_j^{(n)} = \frac{n}{n+1}\left\{v_i^{(n+1)}\left[\delta_{ij} + \delta\tau(\partial_j\mathcal{A}_{ik})\overline{\partial_k S}\right] + \bar{v}_i^{(n+1)}\delta\tau\left[\bar{\mathcal{A}}_{ik}H_{kj} + (\partial_j\mathcal{A}_{ik})\partial_k S\right]\right\} \ , \tag{D.10}
$$

$$
v_j^{(N_\tau)} = \partial_j S(x, N_\tau\delta\tau) \ . \tag{D.11}
$$

Then, the force (D.9) can be obtained as

$$
F_\tau(x, \tau) = \mathrm{Re}\left(f_\tau^{(0)}\right) \ ,
\tag{D.12}
$$

where $f_\tau^{(0)}$ is given by solving

$$
f_\tau^{(n)} = f_\tau^{(n+1)} + \frac{1}{n+1}v_j^{(n+1)}\mathcal{A}_{jk}\overline{\partial_k S} \ , \tag{D.13}
$$

$$
f_\tau^{(N_\tau)} = 0 \ . \tag{D.14}
$$

From (D.10), we find that the computational cost of $O(Q)$ can be avoided by the multi-mass solver here as well.

E The parameters of the GTM used in our simulation

In this appendix, we present the parameters chosen for the GTM such as the range $[\tau_{\min}, \tau_{\max}]$ of the flow time as well as $\tilde{m}$, $m(\tau)$ and $W(\tau)$ that appear in (4.4).

In Table 1, we present the choice of $\tau_{\min}$, $\tau_{\max}$, $\tilde{m}$ and $m(\tau)$, which is parameterized as

$$m(\tau) = \exp\left(\sum_{j=0}^{2} a_j \tau^j\right) \ . \tag{E.1}$$

The symbols O and P in the "flow" column stand for the original and preconditioned flows, respectively[20].

In Table 2, we present the choice of $W(\tau)$, which is parameterized as

$$W(\tau) = \exp(-15\tau) + \sum_{j=1}^{6} b_j \tau^j \ . \tag{E.2}$$

The first term is introduced to avoid the dominance of $\tau = 0$ that occurs otherwise. One can see that the functions $m(\tau)$ and $W(\tau)$ for the preconditioned flow do not have strong dependence on N and x_{f}, which implies that we do not need to fine-tune these functions.

---

[20] For the preconditioned flow with $N = 20$ and $x_{\mathrm{f}} = 0$, the region of τ is chosen to be $[0.4, 0.8]$ in Fig. 4 for the sake of comparison with other values of N, whereas it is chosen to be $[0.6, 1]$ in Fig. 5, which turns out to be more optimal.

Table 1: Parameters for $[\tau_{\min}, \tau_{\max}]$, $\tilde{m}$ and $m(\tau)$

flow	N	x_{f}	$\tau_{\min}$	$\tau_{\max}$	$\tilde{m}$	a_0	a_1	a_2
O	4	0	0.02	0.2	3	-0.362471	9.4008	3.33086
O	6	0	0.02	0.2	3	-0.334801	17.7419	-1.32035
O	8	0	0.02	0.2	3	-0.600957	28.5264	-13.1596
O	10	0	0.02	0.2	4	-0.655057	36.2434	-20.7533
O	12	0	0.02	0.2	4	-0.559024	42.8481	-27.0498
O	14	0	0.02	0.2	4	-0.5425	49.8071	-36.6114
O	16	0	0.02	0.2	5	-0.599934	59.8716	-58.5702
P	4	0	0.4	0.8	1	-0.0309437	1.42644	0.405386
P	6	0	0.4	0.8	1	0.00490622	1.06141	0.671549
P	8	0	0.4	0.8	1	0.0200845	0.72403	1.00223
P	10	0	0.4	0.8	1	-0.0561224	0.930633	0.829279
P	12	0	0.4	0.8	1	-0.178908	1.27849	0.521082
P	14	0	0.4	0.8	1	-0.168445	1.24443	0.531839
P	16	0	0.4	0.8	1	-0.168445	1.24443	0.531839
P	18	0	0.4	0.8	1	-0.126564	1.03928	0.560491
P	20	0	0.4	0.8	1	-0.126564	1.03928	0.560491
P	20	-0.8	0.4	1	1	-0.121107	2.53145	0.158009
P	20	-0.6	0.5	1.1	1	-0.0835431	2.40247	0.228994
P	20	-0.4	0.5	1.1	1	-0.11638	2.56039	0.101282
P	20	-0.2	0.6	1	1	-0.128094	2.54973	0.118526
P	20	0	0.6	1	1	-0.126564	1.03928	0.560491
P	20	0.2	0.9	1.3	1	-0.163594	2.69719	0.00834929
P	20	0.4	0.9	1.3	1	-0.110241	2.42494	0.211641
P	20	0.6	0.8	1.3	1	-0.132109	2.56267	0.0664781
P	20	0.8	0.8	1.3	1	-0.12692	2.4658	0.165435

Table 2: Parameters for $W(\tau)$

flow	N	x_{f}	b_1	b_2	b_3	b_4	b_5	b_6
O	4	0	-91.6818	1328.09	-10070.6	42914.7	-94148.5	82699.2
O	6	0	-73.3069	934.999	-5039.04	15399.9	-25129.1	17155.3
O	8	0	-154.67	2617.17	-17188.6	53938.3	-54440.9	-29989.7
O	10	0	-162.532	3457.74	-27741.1	129678	-367262	516287
O	12	0	86.3215	-907.268	16692.7	-116092	355871	-402478
O	14	0	1464.1	-29301.3	325955	-1942690	5900110	-7172110
O	16	0	6483.54	-144699	1692600	-10685300	34659500	-45355600
P	4	0	-43.3664	161.375	-352.772	437.658	-281.151	72.5656
P	6	0	-43.3664	161.375	-352.772	437.658	-281.151	72.5656
P	8	0	-43.3664	161.375	-352.772	437.658	-281.151	72.5656
P	10	0	-43.3664	161.375	-352.772	437.658	-281.151	72.5656
P	12	0	-43.3664	161.375	-352.772	437.658	-281.151	72.5656
P	14	0	-43.3664	161.375	-352.772	437.658	-281.151	72.5656
P	16	0	-43.3664	161.375	-352.772	437.658	-281.151	72.5656
P	18	0	-43.3664	161.375	-352.772	437.658	-281.151	72.5656
P	20	0	2143.73	-8632.61	18071.1	-20840	12566.2	-3092.1
P	20	-0.8	-93.4087	266.479	-399.747	343.83	-155.337	28.5269
P	20	-0.6	-93.4087	266.479	-399.747	343.83	-155.337	28.5269
P	20	-0.4	-93.7977	266.14	-396.175	336.589	-149.815	27.0416
P	20	-0.2	-89.7574	248.492	-358.03	294.986	-127.833	22.5733
P	20	0	-101.172	250.908	-360.559	300.261	-132.148	23.9199
P	20	0.2	-96.0689	294.63	-466.383	415.773	-193.274	36.3518
P	20	0.4	-105.914	314.982	-488.542	427.174	-194.103	35.5944
P	20	0.6	-103.087	297.241	-447.869	383.163	-171.57	31.2238
P	20	0.8	-93.3297	250.673	-347.381	273.918	-113.639	19.2415

References

[1] J. R. Klauder, *Coherent state Langevin equations for canonical quantum systems with applications to the quantized Hall effect*, Phys. Rev. **A29** (1984) 2036–2047.

[2] G. Parisi, *On complex probabilities*, Phys. Lett. **131B** (1983) 393–395.

[3] E. Witten, *Analytic continuation of Chern-Simons theory*, AMS/IP Stud. Adv. Math. **50** (2011) 347–446, [`arXiv:1001.2933`].

[4] **AuroraScience** Collaboration, M. Cristoforetti, F. Di Renzo, and L. Scorzato, *New approach to the sign problem in quantum field theories: High density qcd on a lefschetz thimble*, Phys.Rev.D **86** (2012) 074506, [`arXiv:1205.3996`].

[5] M. Cristoforetti, F. Di Renzo, A. Mukherjee, and L. Scorzato, *Monte Carlo simulations on the Lefschetz thimble: Taming the sign problem*, Phys. Rev. D **88** (2013), no. 5 051501, [`arXiv:1303.7204`].

[6] H. Fujii, D. Honda, M. Kato, Y. Kikukawa, S. Komatsu, and T. Sano, *Hybrid monte carlo on lefschetz thimbles - a study of the residual sign problem*, JHEP **10** (2013) 147, [`arXiv:1309.4371`].

[7] M. Levin and C. P. Nave, *Tensor renormalization group approach to 2d classical lattice models*, Phys.Rev.Lett. **99** (2007), no. 12 120601, [`cond-mat/0611687`].

[8] Z. Y. Xie, J. Chen, M. P. Qin, J. W. Zhu, L. P. Yang, and T. Xiang, *Coarse-graining renormalization by higher-order singular value decomposition*, Phys. Rev. B **86** (Jul, 2012) 045139.

[9] G. Evenbly and G. Vidal, *Tensor network renormalization*, Phys. Rev. Lett. **115** (Oct, 2015) 180405.

[10] D. Adachi, T. Okubo, and S. Todo, *Anisotropic Tensor Renormalization Group*, Phys. Rev. B **102** (2020), no. 5 054432, [`arXiv:1906.02007`].

[11] D. Kadoh and K. Nakayama, *Renormalization group on a triad network*, `arXiv:1912.02414`.

[12] G. Aarts, E. Seiler, and I.-O. Stamatescu, *The Complex Langevin method: When can it be trusted?*, Phys. Rev. **D81** (2010) 054508, [`arXiv:0912.3360`].

[13] G. Aarts, F. A. James, E. Seiler, and I.-O. Stamatescu, *Complex langevin: Etiology and diagnostics of its main problem*, *Eur.Phys.J.C* **71** (2011) 1756, [arXiv:1101.3270].

[14] K. Nagata, J. Nishimura, and S. Shimasaki, *Justification of the complex Langevin method with the gauge cooling procedure*, *PTEP* **2016** (2016), no. 1 013B01, [arXiv:1508.02377].

[15] K. Nagata, J. Nishimura, and S. Shimasaki, *Argument for justification of the complex Langevin method and the condition for correct convergence*, *Phys. Rev.* **D94** (2016), no. 11 114515, [arXiv:1606.07627].

[16] M. Scherzer, E. Seiler, D. Sexty, and I.-O. Stamatescu, *Complex Langevin and boundary terms*, *Phys. Rev. D* **99** (2019), no. 1 014512, [arXiv:1808.05187].

[17] M. Scherzer, E. Seiler, D. Sexty, and I.-O. Stamatescu, *Controlling Complex Langevin simulations of lattice models by boundary term analysis*, *Phys. Rev. D* **101** (2020), no. 1 014501, [arXiv:1910.09427].

[18] E. Seiler, D. Sexty, and I.-O. Stamatescu, *Complex Langevin: Correctness criteria, boundary terms, and spectrum*, *Phys. Rev. D* **109** (2024), no. 1 014509, [arXiv:2304.00563].

[19] A. Alexandru, G. Basar, P. F. Bedaque, G. W. Ridgway, and N. C. Warrington, *Sign problem and monte carlo calculations beyond lefschetz thimbles*, *JHEP* **05** (2016) 053, [arXiv:1512.08764].

[20] A. Alexandru, G. Basar, P. F. Bedaque, and N. C. Warrington, *Complex Paths Around The Sign Problem*, arXiv:2007.05436.

[21] M. Fukuma and N. Umeda, *Parallel tempering algorithm for integration over lefschetz thimbles*, *PTEP* **2017** (2017), no. 7 073B01, [arXiv:1703.00861].

[22] A. Alexandru, G. Basar, P. F. Bedaque, and N. C. Warrington, *Tempered transitions between thimbles*, *Phys. Rev. D* **96** (2017), no. 3 034513, [arXiv:1703.02414].

[23] M. Fukuma, N. Matsumoto, and N. Umeda, *Implementation of the HMC algorithm on the tempered Lefschetz thimble method*, arXiv:1912.13303.

[24] M. Fukuma and N. Matsumoto, *Worldvolume approach to the tempered Lefschetz thimble method*, *PTEP* **2021** (2021), no. 2 023B08, [arXiv:2012.08468].

[25] M. Fukuma, N. Matsumoto, and Y. Namekawa, *Statistical analysis method for the worldvolume hybrid Monte Carlo algorithm*, *PTEP* **2021** (2021), no. 12 123B02, [`arXiv:2107.06858`].

[26] G. Fujisawa, J. Nishimura, K. Sakai, and A. Yosprakob, *Backpropagating Hybrid Monte Carlo algorithm for fast Lefschetz thimble calculations*, *JHEP* **04** (2022) 179, [`arXiv:2112.10519`].

[27] Y. Tanizaki, H. Nishimura, and J. J. M. Verbaarschot, *Gradient flows without blow-up for Lefschetz thimbles*, *JHEP* **10** (2017) 100, [`arXiv:1706.03822`].

[28] A. Alexandru, G. Basar, P. F. Bedaque, S. Vartak, and N. C. Warrington, *Monte Carlo Study of Real Time Dynamics on the Lattice*, *Phys. Rev. Lett.* **117** (2016), no. 8 081602, [`arXiv:1605.08040`].

[29] A. Alexandru, G. Basar, P. F. Bedaque, and G. W. Ridgway, *Schwinger-Keldysh formalism on the lattice: A faster algorithm and its application to field theory*, *Phys. Rev. D* **95** (2017), no. 11 114501, [`arXiv:1704.06404`].

[30] Z.-G. Mou, P. M. Saffin, A. Tranberg, and S. Woodward, *Real-time quantum dynamics, path integrals and the method of thimbles*, *JHEP* **06** (2019) 094, [`arXiv:1902.09147`].

[31] Z.-G. Mou, P. M. Saffin, and A. Tranberg, *Quantum tunnelling, real-time dynamics and Picard-Lefschetz thimbles*, *JHEP* **11** (2019) 135, [`arXiv:1909.02488`].

[32] S. Woodward, P. M. Saffin, Z.-G. Mou, and A. Tranberg, *Optimisation of Thimble simulations and quantum dynamics of multiple fields in real time*, *JHEP* **10** (2022) 082, [`arXiv:2204.10101`].

[33] J. Nishimura, K. Sakai, and A. Yosprakob, *A new picture of quantum tunneling in the real-time path integral from Lefschetz thimble calculations*, *JHEP* **09** (2023) 110, [`arXiv:2307.11199`].

[34] J. Nishimura, *Quantum tunneling in the real-time path integral by the Lefschetz thimble method*, *PoS* **CORFU2022** (2023) 308, [`arXiv:2308.00345`].

[35] J. Feldbrugge and N. Turok, *Existence of real time quantum path integrals*, *Annals Phys.* **454** (2023) 169315, [`arXiv:2207.12798`].

[36] D. Alvestad, R. Larsen, and A. Rothkopf, *Towards learning optimized kernels for complex Langevin*, *JHEP* **04** (2023) 057, [`arXiv:2211.15625`].

[37] K. Boguslavski, P. Hotzy, and D. I. Müller, *Stabilizing complex Langevin for real-time gauge theories with an anisotropic kernel*, *JHEP* **06** (2023) 011, [`arXiv:2212.08602`].

[38] D. Alvestad, A. Rothkopf, and D. Sexty, *Lattice real-time simulations with learned optimal kernels*, *Phys. Rev. D* **109** (2024), no. 3 L031502, [`arXiv:2310.08053`].

[39] B. Jegerlehner, *Krylov space solvers for shifted linear systems*, `hep-lat/9612014`.

[40] B. Jegerlehner, *Multiple mass solvers*, *Nucl. Phys. B Proc. Suppl.* **63** (1998) 958–960, [`hep-lat/9708029`].

[41] A. D. Kennedy, I. Horvath, and S. Sint, *A New exact method for dynamical fermion computations with nonlocal actions*, *Nucl. Phys. B Proc. Suppl.* **73** (1999) 834–836, [`hep-lat/9809092`].

[42] M. A. Clark, *The Rational Hybrid Monte Carlo Algorithm*, *PoS* **LAT2006** (2006) 004, [`hep-lat/0610048`].

[43] M. A. Clark, A. D. Kennedy, and Z. Sroczynski, *Exact 2+1 flavour RHMC simulations*, *Nucl. Phys. B Proc. Suppl.* **140** (2005) 835–837, [`hep-lat/0409133`].

[44] S. Catterall and T. Wiseman, *Towards lattice simulation of the gauge theory duals to black holes and hot strings*, *JHEP* **12** (2007) 104, [`arXiv:0706.3518`].

[45] K. N. Anagnostopoulos, M. Hanada, J. Nishimura, and S. Takeuchi, *Monte Carlo studies of supersymmetric matrix quantum mechanics with sixteen supercharges at finite temperature*, *Phys. Rev. Lett.* **100** (2008) 021601, [`arXiv:0707.4454`].

[46] S.-W. Kim, J. Nishimura, and A. Tsuchiya, *Expanding (3+1)-dimensional universe from a Lorentzian matrix model for superstring theory in (9+1)-dimensions*, *Phys. Rev. Lett.* **108** (2012) 011601, [`arXiv:1108.1540`].

[47] M. Fukuma, *Simplified algorithm for the Worldvolume HMC and the Generalized-thimble HMC*, `arXiv:2311.10663`.

[48] J. Feldbrugge, D. L. Jow, and U.-L. Pen, *Crossing singularities in the saddle point approximation*, `arXiv:2309.12427`.